Absorption-Ablation-Excitation Mechanism of Laser-Cluster Interactions in a Nanoaerosol System

Yihua Ren,[1] Shuiqing Li,[1,*] Yiyang Zhang,[2] Stephen D. Tse,[3] and Marshall B. Long[4]
[1]*Key Laboratory for Thermal Science and Power Engineering of Ministry of Education, Department of Thermal Engineering, Tsinghua University, Beijing 100084, China*
[2]*Collaborative Innovation Center of Advanced Nuclear Energy Technology, Institute of Nuclear and New Energy Technology, Tsinghua University, Beijing 100084, China*
[3]*Department of Mechanical and Aerospace Engineering, Rutgers, The State University of New Jersey, Piscataway, New Jersey 08854, USA*
[4]*Department of Mechanical Engineering & Materials Science, Yale University, New Haven, Connecticut 06520, USA*
(Received 12 July 2014; published 5 March 2015)

The absorption-ablation-excitation mechanism in laser-cluster interactions is investigated by measuring Rayleigh scattering of aerosol clusters along with atomic emission from phase-selective laser-induced breakdown spectroscopy. For 532 nm excitation, as the laser intensity increases beyond 0.16 GW/cm^2, the scattering cross section of TiO_2 clusters begins to decrease, concurrent with the onset of atomic emission of Ti, indicating a scattering-to-ablation transition and the formation of nanoplasmas. With 1064 nm laser excitation, the atomic emissions are more than one order of magnitude weaker than that at 532 nm, indicating that the thermal effect is not the main mechanism. To better clarify the process, time-resolved measurements of scattering signals are examined for different excitation laser intensities. For increasing laser intensity, the cross section of clusters decreases during a single pulse, evincing the shorter ablation delay time and larger ratios of ablation clusters. Assessment of the electron energy distribution during the ablation process is conducted by nondimensionalizing the Fokker-Planck equation, with analogous Strouhal Sl_E, Peclet Pe_E, and Damköhler Da_E numbers defined to characterize the laser-induced aerothermochemical environment. For conditions where $Sl_E \gg 1$, $Pe_E \gg 1$, and $Da_E \ll 1$, the electrons are excited to the conduction band by two-photon absorption, then relax to the bottom of the conduction band by electron energy loss to the lattice, and finally serve as the energy transfer media between laser field and lattice. The relationship between delay time and excitation intensity is well correlated by this simplified model with quasisteady assumption.

DOI: 10.1103/PhysRevLett.114.093401 PACS numbers: 36.40.Gk, 52.25.Os, 52.38.Mf, 78.47.je

Laser-cluster interactions are widespread across fundamental physical processes in many disciplines. Depending on the excitation laser intensity, such interactions can be used for characterization of particles or aggregates based on elastic and inelastic scattering (10^2–10^8 W/cm^2) [1–4], determination of local chemical compositions based on laser-induced breakdown or aerosol-fragmentation spectroscopy (10^8–10^{12} W/cm^2) [5–8], and investigation of laser-driven nonlinear clusters dynamics based on a generation of energetic photons and x rays (10^{11}–10^{18} W/cm^2) [9–15]. For scattering-to-breakdown transition, the generally accepted mechanism involves the production of initial electrons from multiphoton excitation or tunnel ionization (distinguished by the Keldysh adiabaticity parameter [10,16]), followed by fast production of electrons due to cascade collisional ionization (inverse bremsstrahlung) and the emergence of shock wave(s) by hydrodynamic or Coulombic expansion. In practice, the breakdown threshold is defined by the excitation laser intensity at which the transmitted laser intensity decreases and the emission of bremsstrahlung radiation forms. Recently, a new phase-selective laser-induced breakdown spectroscopy (PS-LIBS) has been developed for the diagnosis of gas-to-particle transition at nanoscale [17,18]. The PS-LIBS excites only constituent atoms (e.g., Ti in TiO_2) in the particle phase, with no breakdown emission occurring for surrounding gas molecules, presenting a robust technique for cluster or nanoparticle identification, monitoring, and concentration mapping for many aerosol systems. Spatially localized nanoplasmas are found around individual TiO_2 nanoparticles, without macroscopic sparks or bremsstrahlung radiation, while atomic emissions are detected, suggesting a novel laser-cluster interaction mechanism between the scattering and breakdown regimes.

Such localized nanoplasmas formed around nanoparticles in PS-LIBS are believed to be produced through ablation of the clusters. The ablation-driven laser-cluster interaction differs significantly from the laser-induced damage of solid materials and microsized particles because (i) impact ionization (inverse bremsstrahlung heating) is negligible due to the rare diffusion of electrons to higher energy levels [19], (ii) avalanching explosive vaporization on the surface of microparticles has not been observed [20], and (iii) direct photon-phonon coupling is not the main mechanism. Moreover, the novel interaction mechanism is different from those where intense laser photons strike van

der Waals crystal clusters given the quasisteady feature of the ablation process and the lack of hydrodynamic or Coulombic expansion due to the small multiphoton ionization rates of electrons [10]. Similar ablation phenomena have also been observed in laser-induced incandescence of soot [21] and metal oxide clusters [22,23], with direct laser heating dominating. Such studies focused on the removal of material and thermal radiation from particles. Li *et al.*[24] and Lucas *et al.*[8] proposed that lattice defects or surface excitons facilitate electronic excitation with photons of subband-gap energy in their investigations on the photo fragmentation of wide-band-gap particles by UV light. However, for the weak ablation of narrow-band-gap semiconductor clusters without shock wave ahead of ejected species, a clearer physical picture is needed to better understand this laser-cluster interaction regime.

Here, the absorption-ablation-excitation mechanism in PS-LIBS is investigated by examining Rayleigh scattering and atomic emissions from clusters, with further analysis of a dimensionless Fokker-Planck equation. The physical mechanism involved in PS-LIBS is illustrated in Fig. 1, along with the experimental setup. The laser intensity at the scattering-to-ablation transition point is clearly identified by the reduction of scattering cross sections of clusters and the onset of atomic emissions. The ablation delay time can be deduced by time-resolved scattering measurements, and can be modeled by appropriately nondimensionalizing the Fokker-Planck equation.

The experimental setup is similar with that employed in our recent work [18], with the schematic shown in Fig. 1(d) and more details given as Supplemental Material [25]. Flame-synthesized nanoclusters have a mean diameter of 11 nm, and a number density $\sim 10^{11}\#/\mathrm{cm}^3$, which ensures the statistical significance of the measurements. The 532/1064 nm laser beam is focused on the axial centerline of the cluster-laden flow field at 21 mm above the burner exit. The signals are collected into an Acton-SpectraPro-300i spectrometer and detected by a PI-MAX3 ICCD camera. The ICCD gate width is set to 200–600 ns for measuring the integrated Rayleigh scattering signal and then set to 2.54 ns for successive time-shifted measuring of the temporal evolution of the scattering. A series of neutral-density filters are placed upstream of the beam-focusing lens to adjust the excitation laser intensity with little change to the profile and delay time of the laser pulse.

Scattering intensity, scattering efficiency, and atomic emission of clusters for varying excitation laser intensity are shown in Fig. 2. The net scattering response of 532 nm excitation from clusters can be obtained by subtracting scattering signals of nanoaerosols (gas + cluster) from that of pure gases (gas). The flame environment does not change with or without clusters, ensuring the same gas Rayleigh cross sections for the two situations. The scattering intensity of clusters first increases proportionally with the intensity of 532 nm laser excitation, and then flattens out, while the scattering intensity of pure gases is linear with laser intensity, for the same range, as depicted in the inset of Fig. 2. The scattering efficiency of clusters, defined as the ratio of the scattering signal intensity to the laser intensity, is approximately constant up to 0.8 mJ/pulse (0.16 $\mathrm{GW/cm}^2$), and then begins to decrease after this critical value, showing the same tendency of scattering cross section and demarcating the onset of laser ablation of the clusters. Above the ablation threshold for these conditions, the atomic emission from Ti atoms excited by 532 nm laser, i.e., from PS-LIBS, is observed, further corroborating the formation of nanoplasmas upon ablation. The atomic spectrum of Ti near 500 nm is

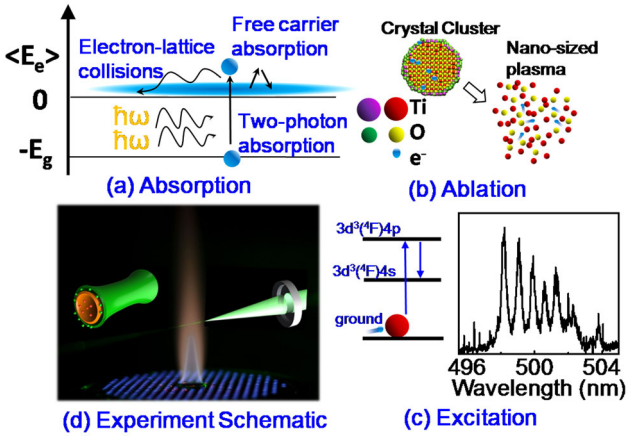

FIG. 1 (color online). Schematic of (a)–(c) the absorption-ablation-excitation mechanism and (d) the experiment setup. In panel (a), the electrons are excited to the conduction band by two-photon absorption, then return to the bottom of the conduction band by electron energy loss and transfer energy from laser to lattice. The ablated clusters then transform into a nanoplasma, as depicted in panel (b). Finally, the electrons in the plasma excite the atoms producing atomic emission, as shown in panel (c).

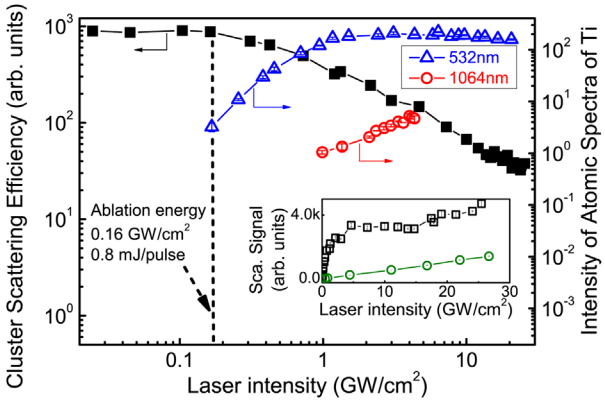

FIG. 2 (color online). Scattering efficiency of TiO_2 clusters with 532 nm laser excitation (black squares) and atomic emission intensity of titanium at 498.17 nm with 532 nm laser (blue triangles) and 1064 nm laser excitation (red circles) at different laser intensities. The scattering efficiency of clusters with 532 nm laser excitation is defined as the ratio of the scattering signal intensity to the laser intensity. The inset shows the comparison of scattering signals of clusters (black squares) and gases (green circles) with 532 nm laser excitation.

shown in the plot of Fig. 1(c). It should be noted that the first appearance of atomic emission of Ti at the wavelength of 498.17 nm (corresponding to the transition of electronic energy level $3d^3 4s$ to $3d^3 4p$) occurs exactly at the same laser intensity as when clusters' cross sections start to decrease, demonstrating that the PS-LIBS signal is caused by the ablation of clusters. The atomic emission intensities saturate after 1 GW/cm^2, implying that the number of electrons after ablation plateaus at strong laser intensity, which will be discussed later.

The ablation process is further investigated by changing the excitation laser wavelength to 1064 nm (red circles in Fig. 2), to examine the role of the conventional thermal effect. Under the same flame conditions, atomic emission occurs when the 1064 nm laser intensity exceeds an onset intensity of 1 GW/cm^2, which is about 6 times higher than that for the 532 nm case. Meanwhile, the atomic emission with the 1064 nm laser excitation is much weaker—about 1 to 2 orders of magnitude lower than that for 532 nm excitation with the same intensity. The laser intensity is kept below 4.5 GW/cm^2 because tiny sparks from breakdown are observed at high intensities. Since photons with longer wavelength are more likely to interact thermally with vibrational modes of the nanoparticles, the much weaker atomic emissions and their higher onset threshold at 1064 nm laser excitation clarify that direct photon-phonon thermal coupling is not the main mechanism in the ablation process of PS-LIBS.

The ablation process of clusters with 532 nm laser excitation is further examined by time-resolved Rayleigh scattering measurements, as shown in Fig. 3. The time-resolved scattering intensities of both gases and clusters are normalized with respect to maximum intensity. The starting relative time of the temporal evolution of the signals is set to zero, concurrent with an incoming laser pulse, i.e., the initial occurrence of the gas Rayleigh signal. When the laser intensities are below the ablation threshold, as seen in Figs. 3(a) and 3(b), the Rayleigh scattering of clusters (black triangles) is nearly synchronous with the gas Rayleigh signal (fitted by Gaussian functions shown as solid red curves), revealing an elastic response of the clusters to the laser pulse. When the laser intensities exceed the ablation threshold, the scatterings or emissions of clusters significantly deviate from that for pure gas, displaying an obvious drop after the first few nanoseconds, before increasing again. The drop points of the scattering curves indicate the reduction of cross sections, i.e., the scattering-to-ablation transition during the laser pulse. The atomic spectrum of Ti also appears at this instant. Therefore, the signals before the transition point come from the scattering response of clusters, while after that, they come from scattering of ablated fragments. To quantify fragmentation degree, the scatterings of clusters before the transition moment are fitted with a Gaussian function (i.e., red dashed curve). The fragmentation degree during ablation can be assessed by the vertical gap between the cluster Gaussian curve and the scattering signals from the ablated fragments, which increases with laser intensity, consistent with the decrease of integrated cross sections at larger laser intensities as shown in Fig. 2. The ablation delay time, which is marked in Fig. 3 as the obvious dropping point of cluster scattering, becomes shorter with increasing laser intensity for the range examined.

According to semiconductor absorption theory [28], the direct absorption of 2.34 eV photon by TiO_2 nanoparticles is difficult because (i) the photon energy is below the 3.2 eV band gap, (ii) the lattice absorption region is located in the infrared spectrum, and (iii) the surface effect does not enhance the absorption of 532 nm light significantly [29].

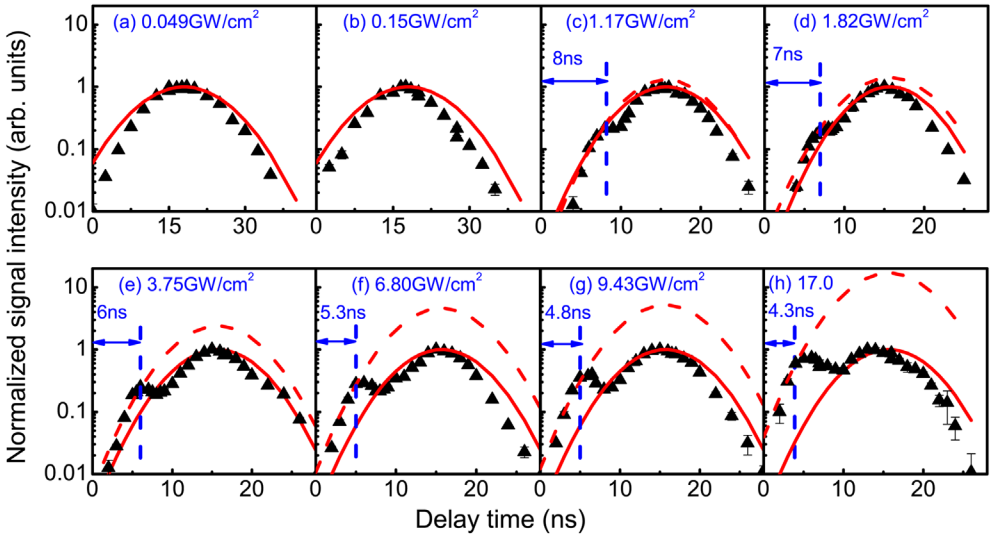

FIG. 3 (color online). Time-resolved measurements of scattering signals of clusters (black triangles) and Gaussian fitting of Rayleigh scatterings (red curves) at different laser intensities. The elastic scatterings of clusters before the transition moment are fitted by Gaussian curves (dashed red curve), which extrapolate beyond the transition moment, with similar profiles but different magnitudes compared to the normalized gas Rayleigh curves (solid red curve).

The weak atomic emissions from 1064 nm laser excitation further confirm that the ablation process is not caused by direct photon-phonon coupling. Therefore, conduction-band electrons from multiphoton excitation are believed to be responsible for the ablation process. The energy distribution of electrons can be described by the Fokker-Planck equation [19,30], i.e., the convection-diffusion equation in energy space:

$$\frac{\partial}{\partial t}f(u,t)=\frac{\partial}{\partial u}\left[(B_{u,t}-A_{u,t})f(u,t)+D_{u,t}\frac{\partial f(u,t)}{\partial u}\right]+S, \tag{1}$$

where $f(u,t)du$ is the number of electrons with energy between u and $u+du$ at time t in one cluster, and $S=S_{\mathrm{MPI}}+S_{\mathrm{imp}}$ represents the sources and sinks of electrons considering multiphoton excitation and impact ionization. (The recombination term can be neglected given the relatively large band gap of 3.2 eV for TiO_2 considered here.) The first term on the right is the net number of electrons across an energy value u per unit time, including the convection and diffusion of conduction-band electrons in energy space. The convection term contains the rate of absorption of electromagnetic energy by electrons via collisions, i.e., joule heating rate $A_{u,t}$, and the rate of electron energy loss to the lattice $B_{u,t}$ for which the formulas are presented in detail in Refs. [19,30–32]. The Fokker-Planck equation can be nondimensionalized to the form

$$\frac{\partial f^*}{\partial t^*}\frac{t_{\mathrm{conv}}}{t_{\mathrm{laser}}}=\frac{\partial}{\partial u^*}\left(f^*+\frac{t_{\mathrm{conv}}}{t_{\mathrm{diff}}}\frac{\partial f^*}{\partial u^*}\right)+\frac{t_{\mathrm{conv}}}{t_{\mathrm{react}}}F_{\mathrm{mpi}}(u^*), \tag{2}$$

where t_{laser} is the time scale of the laser pulse (~10 ns), $t_{\mathrm{conv}}=E_{bg}/(B\text{-}A)$ is the convection time (10^{-7}–10^{-6} ns), $t_{\mathrm{diff}}={E_{bg}}^2/D$ is the diffusion time (0.1–10^2 ns), $t_{\mathrm{react}}=2h\nu/\beta I^2 V_p$ is the excitation time of two-photon absorption (10^{-6}–1 ns) which is strongly dependent on the laser intensity from 0.02–20.4 GW/cm^2 (β is the two-photon absorption coefficient, I is the laser intensity, $h\nu$ is the photon energy), $f^*=fE_{bg}$ is a nondimensional distribution function of electron number in one cluster, and $F_{\mathrm{mpi}}(u^*)$ is a nondimensional function that describes the energy distribution of electrons generated from multiphoton ionization. The Strouhal number Sl_E, defined as $t_{\mathrm{laser}}/t_{\mathrm{conv}}$ (analogous to that defined in fluid dynamics) [33], expresses the ratio of the intrinsic time scale to the convective time scale and is about 10^7–10^8. Thus the whole ablation process reaches quasi-steady state. The Peclet number Pe_E, defined as $t_{\mathrm{diff}}/t_{\mathrm{conv}}$, is about 10^5–10^9. Thus diffusion of conduction-band electrons in energy space can be neglected, and impact ionization by diffused electrons to higher energies is not considered here. The dimensionless reaction parameter Da_E, defined as $t_{\mathrm{conv}}/t_{\mathrm{react}}$ (analogous to the Damköhler number in combustion systems [34]), ranges from ~10^{-6} (weak laser intensity 0.02 GW/cm^2) to ~1 (strong laser intensity 20.4 GW/cm^2).

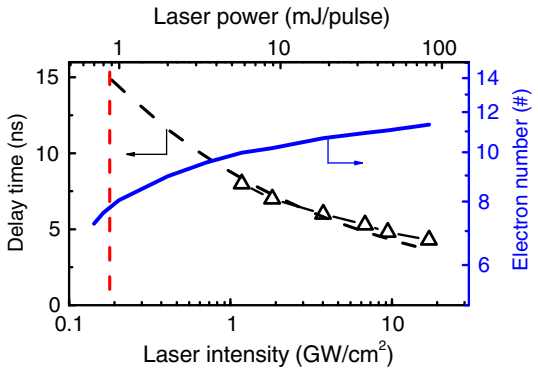

FIG. 4 (color online). The ablation durations at different laser intensities are denoted by the black line (model result) and the symbols (time-resolved measurements). At the minimum ablation laser intensity, which is marked by the red dashed line, the delay time of ablation is about the same as the duration of the laser pulse. The modeled electron number is characterized by the blue dashed line, which increases and saturates with increasing laser intensity.

At moderate values of laser intensity, electrons relax to the bottom of the conduction band after two-photon excitation. For $\mathrm{Sl}_E \gg 1$, $\mathrm{Pe}_E \gg 1$, and $\mathrm{Da}_E \ll 1$ conditions, the electrons are excited to the conduction band by two-photon absorption, and return to the bottom of the conduction band by electron energy loss via collisions with the lattice, as previously described and depicted in Fig. 1(a). This absorption-ablation-excitation laser-cluster interaction is different from conventional laser-induced breakdown and intense laser-cluster interaction. For the conventional laser-induced breakdown regime, diffusion of electrons to a higher energy level contributes to impact ionization, and thus Pe_E reaches 1 [19]. While for the intense laser-cluster interaction regime, the assumption of $\mathrm{Sl}_E \gg 1$ is invalid due to the ultrashort laser pulse (e.g., femtosecond) [10]; and the whole process cannot be regarded as quasisteady state. For the laser induced fragmentation of metal particles, a large source of nearly free electrons leads to $\mathrm{Da}_E \gg 1$ [35].

Based on the above analysis, a simplified ablation model is proposed with the assumption that all the conduction-band electrons N are created by two-photon excitation:

$$\frac{\partial N}{\partial t}=\frac{\beta I^2 V_p}{2h\nu}. \tag{3}$$

The cluster lattice is heated to vaporization by joule heating from conduction-band electrons under an electric field with the power of AN. The clusters are ablated in shorter time for stronger laser field due to faster production of conduction-band electrons and stronger joule heating, which is observed in the time-resolved measurement and well predicted by the model, as shown in Fig. 4. The small deviation at large laser intensities may be caused by the less rigorous assumption of $\mathrm{Da}_E \ll 1$ and the possibility that not all the electrons are at the bottom of the conduction band. At the minimum ablation laser intensity (~0.16 GW/cm^2), as denoted by the vertical

red dashed line, the delay time of ablation is about the same as the laser pulse duration. Below this intensity threshold, the time required for ablating particles is even longer than the laser pulse duration, which makes ablation incomplete. As the laser intensity increases, the number of free electrons first increases and then tends to saturate (blue line in Fig. 4). This saturation trend of electron numbers can partially explain the saturation of Ti atomic emission with increasing laser intensity, as given in Fig. 2. Further interpretation needs a complete knowledge of the electron energy distribution in the ablation-formed nanoplasmas, which is beyond the scope of this Letter.

In summary, temporal Rayleigh scattering measurements and atomic emissions from 532/1064 nm laser excitation, together with the model derived from the Fokker Planck equation, divulge a new regime of laser-cluster interaction. Both the scattering signals and the atomic emissions point to the occurrence of ablation of clusters at an onset laser intensity of about 0.16 GW/cm^2. With time-resolved data and dimensional analysis, the physical mechanism of TiO_2 nanoparticle ablation is clarified, where electrons are first excited to the conduction band by two-photon absorption, then return to the bottom of the conduction band by collisional loss to the lattice, and finally become the energy transfer media between the laser field and the lattice. For conditions of $Sl_E \gg 1$, $Pe_E \gg 1$, and $Da_E \ll 1$, this interaction between weak intensity laser and semiconductor clusters is believed to be novel and distinct from conventional LIBS, laser-induced incandescence, and laser induced fragmentation.

This research is supported by the National Natural Science Funds of China (Grant No. 51176094) and the National Key Basic Research and Development Program (Grant No. 2013CB228506). S. Q. L. acknowledges the China Scholarship Council for his time at Yale and Princeton, as well as Professor Michael Renfro at Connecticut, Professor Hai Wang at Stanford and Professors Qiang Yao and Yikang Pu at Tsinghua for discussions.

*Corresponding author.
lishuiqing@tsinghua.edu.cn

[1] Y. Xing, U. O. Koylu, and D. E. Rosner, Appl. Opt. **38**, 2686 (1999).
[2] D. R. Snelling, O. Link, K. A. Thomson, and G. J. Smallwood, Appl. Phys. B **104**, 385 (2011).
[3] G. Yang and P. Biswas, Aerosol Sci. Technol. **27**, 507 (1997).
[4] M. J. Berg, S. C. Hill, Y.-L. Pan, and G. Videen, Opt. Express **18**, 23343 (2010).
[5] Y. A. Yang, P. Xia, A. L. Junkin, and L. A. Bloomfield, Phys. Rev. Lett. **66**, 9 (1991).
[6] D. W. Hahn and N. Omenetto, Appl. Spectrosc. **64**, 335 (2010).
[7] D. S. Thomson and D. M. Murphy, Appl. Opt. **32**, 6818 (1993).
[8] J. H. Choi, C. B. Stipe, C. P. Koshland, R. F. Sawyer, and D. Lucas, J. Appl. Phys. **97**, 124315 (2005).
[9] T. V. Liseykina and D. Bauer, Phys. Rev. Lett. **110**, 145003 (2013).
[10] T. Fennel, K.-H. Meiwes-Broer, J. Tiggesbäumker, P.-G. Reinhard, P. M. Dinh, and E. Suraud, Rev. Mod. Phys. **82**, 1793 (2010).
[11] U. Saalmann, C. Siedschlag, and J. M. Rost, J. Phys. B **39**, R39 (2006).
[12] C. Bostedt, E. Eremina, D. Rupp, M. Adolph, H. Thomas, M. Hoener, A. R. B. de Castro, J. Tiggesbäumker, K.-H. Meiwes-Broer, T. Laarmann, H. Wabnitz, E. Plönjes, R. Treusch, J. R. Schneider, and T. Möller, Phys. Rev. Lett. **108**, 093401 (2012).
[13] F. Dorchies, F. Blasco, C. Bonté, T. Caillaud, C. Fourment, and O. Peyrusse, Phys. Rev. Lett. **100**, 205002 (2008).
[14] T. Fennel, L. Ramunno, and T. Brabec, Phys. Rev. Lett. **99**, 233401 (2007).
[15] T. Ditmire, T. Donnelly, A. M. Rubenchik, R. W. Falcone, and M. D. Perry, Phys. Rev. A **53**, 3379 (1996).
[16] L. V. Keldysh, Sov. Phys. JETP **20**, 1307 (1965).
[17] Y. Zhang, G. Xiong, S. Li, Z. Dong, S. G. Buckley, and S. D. Tse, Combust. Flame **160**, 725 (2013).
[18] Y. Zhang, S. Li, Y. Ren, Q. Yao, and C. K. Law, Appl. Phys. Lett. **104**, 023115 (2014).
[19] L. H. Holway, Jr., J. Appl. Phys. **45**, 677 (1974).
[20] S. Atutov, W. Baldini, V. Biancalana, R. Calabrese, V. Guidi, B. Mai, E. Mariotti, G. Mazzocca, L. Moi, S. Pod'yachev, and L. Tomassetti, Phys. Rev. Lett. **87**, 215002 (2001).
[21] N.-E. Olofsson, J. Johnsson, H. Bladh, and P.-E. Bengtsson, Appl. Phys. B **112**, 333 (2013).
[22] Y. Murakami, T. Sugatani, and Y. Nosaka, J. Phys. Chem. A **109**, 8994 (2005).
[23] S. Maffi, F. Cignoli, C. Bellomunno, S. De Iuliis, and G. Zizak, Spectrochim. Acta B Atom. Spectros. **63**, 202 (2008).
[24] X. Li, R. D. Beck, and R. L. Whetten, Phys. Rev. Lett. **68**, 3420 (1992).
[25] See Supplemental Material at http://link.aps.org/supplemental/10.1103/PhysRevLett.114.093401, which includes Refs. [26,27], for the description of the experimental setup and the derivation of the Fokker-Planck equation.
[26] G. Hartung, J. Hult, and C. F. Kaminski, Meas. Sci. Technol. **17**, 2485 (2006).
[27] Y. Zhang, S. Li, Y. Ren, Q. Yao, and S. D. Tse, Proc. Combust. Inst. **35**, 3681 (2015).
[28] M. V. Allmen, *Laser-Beam Interactions with Materials* (Springer, Berlin, 1987).
[29] K. Madhusudan Reddy, C. V. Gopal Reddy, and S. V. Manorama, J. Solid State Chem. **158**, 180 (2001).
[30] M. Sparks, D. L. Mills, R. Warren, T. Holstein, A. A. Maradudin, L. J. Sham, E. Loh Jr., and D. F. King, Phys. Rev. B **24**, 3519 (1981).
[31] H. B. Callen, Phys. Rev. **76**, 1394 (1949).
[32] H. Fröhlich, Proc. R. Soc. A **160**, 230 (1937).
[33] A. Prosperetti and G. Tryggvason, *Computational Methods for Multiphase Flow* (Cambridge University Press, Cambridge, 2009).
[34] C. K. Law, *Combustion Physics* (Cambridge University Press, New York, 2006).
[35] R. K. Raman, R. A. Murdick, R. J. Worhatch, Y. Murooka, S. D. Mahanti, T-R. T. Han, and C-Y. Ruan, Phys. Rev. Lett. **104**, 123401 (2010).